

pubs.acs.org/ac Article

Optimized Sawhorse Waveform for the Measurement of Oxytocin Release in Zebrafish

Romana Jarosova, Adam D. Douglass, and Michael A. Johnson*

Metrics & More



ACCESS I



Article Recommendations

OXT NH OH ON OXT NH OH OH OXT NH OH OXT NH OH OXT NH OXT N

ABSTRACT: Oxytocin is a nonapeptide hormone involved in numerous physiological functions. Real-time electrochemical measurements of oxytocin in living tissue are challenging due to electrode fouling and the large potentials needed to oxidize the tyrosine residue. Here, we used fast-scan cyclic voltammetry at carbon-fiber microelectrodes and flow injection analysis to optimize a waveform for the measurement of oxytocin. This optimized waveform employed an accumulation potential of -0.6 V, multiple scan rates, and a 3 ms holding potential at a positive, oxidizing potential of +1.4 V before linearly scanning the potential back to -0.6 V (versus Ag/AgCl). We obtained a limit of quantitation of $0.34 \pm 0.02 \,\mu\text{M}$, and our electrodes did not foul upon multiple injections. Moreover, to demonstrate the utility of our method, we measured the release of oxytocin, evoked by light application and mechanical perturbation, in whole brains from genetically engineered adult zebrafish that express channelrhodopsin-2 selectively on oxytocinergic neurons. Collectively, this work expands the toolkit for the measurement of peptides in living tissue preparations.

xytocin is a nonapeptide hormone that acts as an endocrine chemical messenger, playing roles in numerous functions, including parturition, lactation, pair-bonding, maternal care, sexual behavior, social attachment, and the relief of fear and anxiety. In the mammalian brain, oxytocin is synthesized mainly in the hypothalamic periventricular nucleus (PVN) and the magnocellular hypothalamic supraoptic nucleus (SON).^{6,8–10} Oxytocin influences the release of multiple neurotransmitters, including dopamine, 11 serotonin, 12 and GABA¹³ through its interactions with receptors in several brain regions, including the thalamus, hypothalamus, brainstem, basal ganglia, limbic system, and select cortical areas. 9,14 Thus, given its specific functions in regulating neurotransmitter systems, understanding the dynamics of oxytocin release on relevant timescales and with sufficient sensitivity in living brain tissue is a critical need.

Current methods of measuring oxytocin in living brain described in the primary literature are limited mostly to sampling approaches, including microdialysis¹⁵ and push—pull perfusion,¹⁶ used in conjunction with select detection schemes, such as radioimmunoassay (RIA),¹⁶ derivatization and fluorescence detection,¹⁷ and mass spectrometry.^{18,19} While

these sampling methods have the advantage of analyzing a wide variety of molecule types, the temporal resolution is limited by the amount of material collected, and usually is on the order of minutes. Another detection method employed molecularly imprinted polymers (MIPs) with quartz crystal microbalance (QCM); however, the utility of this method for the measurement of oxytocin in microdialysate samples has not yet been demonstrated.

Supporting Information

Electrochemical methods represent a potentially fruitful avenue for measuring oxytocin with a subsecond timescale resolution. However, the electrochemical measurement of oxytocin can be challenging. Although the tyrosine residue in oxytocin is electroactive, it has been previously reported that the oxidation of tyrosine-containing neuropeptides tends to

Received: November 9, 2021 Accepted: January 21, 2022 Published: February 2, 2022





foul the electrode surface due to adsorption of oxidized or polymerized protein molecules, causing low reproducibility. ^{22,23} Additionally, there is a need for a higher oxidation potential in comparison with traditionally detected molecules (*e.g.*, catecholamines), which leads to additional problems with interferents. ²⁴ To overcome these limitations, Schmidt et al. ²³ designed a modified sawhorse waveform (MSW), consisting of two distinct scan rates in each anodic and cathodic sweep, and a short holding period at the switching potential. This approach, termed multiple scan rate voltammetry (MSRV), not only mitigates electrode fouling but also improves chemical resolution in the detection of tyrosine-containing peptides. ^{23,25}

Despite growing interest, many functional aspects of oxytocin in the brain have not yet been fully described due largely to the lack of analytical tools that allow its quantitative measurement in intact tissue on fast (subsecond) timescales. Here, we adapted MSRV to measure oxytocin through the oxidation of the tyrosine residue. Our results show that we can quantitatively measure oxytocin in a flow cell with good limits of detection and subsecond temporal resolution. Furthermore, we demonstrated the feasibility of our method by measuring the light-evoked release of oxytocin in live, intact whole brains acutely harvested from zebrafish engineered to express channelrhodopsin on oxytocin-containing neurons. In this model, exposure of oxytocinergic neurons to light of the proper wavelength can induce the release of oxytocin. Additionally, we demonstrated that the release of oxytocin may be induced by mechanical stimulation of the brain tissue.

EXPERIMENTAL SECTION

Chemicals. All chemicals were purchased from Sigma-Aldrich (St. Louis, MO) and used as received. A stock solution of 20 μ M oxytocin (CAS no. 50-56-6, \geq 97.0%) was prepared by dissolving the appropriate amount of analyte in artificial cerebrospinal fluid (aCSF; 126 mM NaCl, 2.5 mM KCl, 1.2 mM NaH₂PO₄, 2.4 mM CaCl₂, 1.2 mM MgCl₂, 25 mM NaHCO₃, and 20 mM HEPES, adjusted to pH 7.4 with 10 M NaOH). The solutions used for generating the calibration curves were prepared by serial dilution on the stock solution. The stock solution was stored at 5 °C in the dark and used within 48 h of preparation. All solutions were made using ultrapure water (\sim 18 M Ω cm).

Microelectrode Fabrication. Carbon-fiber working electrodes were constructed following the previously published procedure.²⁶ Briefly, a 7 µm diameter carbon fiber (Goodfellow Cambridge Ltd., Huntingdon, U.K.) was aspirated into a glass capillary tube (1.2 mm outer diameter, 0.68 mm inner diameter, A-M system, Inc., Carlsborg, WA) and fixed in the position by sealing the glass capillary around the fiber using a heated coil puller (PE-22, Narishige Int., East Meadow, NY). Next, the exposed carbon fiber was trimmed to approximately 40 μ m from the end of pulled glass capillary, and an epoxy seal was created (EPON resin 815C, EPIKURE 3234 curing agent, Miller-Stephenson, Danbury, CT). The microelectrode was further cured at 100 °C for 1 h and cleaned by soaking in ultrapure isopropanol for 30 min. To ensure electrical connection between the carbon fiber and electrode holder, all electrodes were backfilled by ionic solution (0.5 M potassium acetate) and a silver wire was inserted.

Electrochemical Data Acquisition *In Vitro*. All *in vitro* experiments were carried out in a homemade flow injection cell, housed within a custom-built faraday cage. A Chem Clamp potentiostat (Dagan, Minneapolis, MN) modified to

enhance the range of available gain settings was used. TarHeel CV software (M.L.A.V. Heien and R.M. Wightman, University of North Carolina, Chapel Hill, NC) with data acquisition PCI 6711 multifunction I/O board (National Instruments, Austin, TX) was used to collect and analyze all data. The modified sawhorse waveform (MSW) 23,25 was originally used and further optimized. Specifically, the waveform started at a holding potential of -0.2 V and scanned to +0.6 at 100 V/s. Then, the potential was ramped to +1.2 V at 400 V/s and held for 3 ms. Finally, the potential was scanned back to -0.2 V at a scan rate of 100 V/s, at a frequency of 10 Hz.

Animals. Zebrafish embryos Danio rerio, transgenic line Tg(oxt:Gal4-VP16; uas:chr2-eyfp) were raised until adulthood (~90 days). The fish were housed in the Shankel Structural Biology Center, University of Kansas, in 3 L tanks (20 fish per 3 L system rack tank) and connected to a recirculation filtration system. All tanks were maintained under constant chemical, biological, and mechanical filtration, as well as a UV sterilizing unit to ensure adequate conditions. The following quality parameters of the reverse osmosis purified system water were controlled and adjusted using Multiparameter Monitoring and Control Instrument 5200A (YSI, Yellow Springs, OH): conductivity ($\sim 700 \ \mu\text{S/cm}$), pH (7.2), and temperature (28 °C). The fish were fed twice a day and maintained on a 14:10 h light/dark cycle. All protocols and procedures involving zebrafish were approved by the Animal Care and Use Committee of the University of Kansas.

Electrochemical Detection of Oxytocin in Zebrafish Whole Brain. All zebrafish were euthanized by hypothermic shock followed by decapitation. Immediately following euthanasia, whole brains were harvested using previously described methods²⁶ and transferred to a superfusion chamber. The viability of the brain was ensured by a continuous flow of oxygenated and heated (28 °C) aCSF. Prior to any experiment, the brain was equilibrated in the chamber for 40 min. The carbon-fiber microelectrode was positioned into the preoptic area of the hypothalamus where epifluorescence imaging showed dense oxytocinergic innervation. Oxytocin in zebrafish is also known as isotocin and differs slightly in amino acid composition compared to mammalian oxytocin.²⁷

For the optogenetics activation of cells, ADD created the UAS line using the H134R variant of ChR2, which was originally described. The peak excitation is ~460 nm, which may vary slightly depending on where it is expressed and pH. ChR2 is expressed only in oxytocinergic neurons, which has previously been verified. Habient light generally contains insufficient blue light to activate cells expressing this ChR2 variant. However, experiments were performed in the dark as a precaution. For stimulated release measurements, light from a xenon source (~480 nm) was applied for 200 ms and the oxidation current was used against a calibration to determine concentration.

Microscopy. Epifluorescence images were obtained with a Nikon E600FN Epifluorescence microscope using a Fluor 40X/0.80 NA water immersion objective. Images were collected and analyzed with Metamorph software (Molecular Devices, San Jose, CA).

Statistics and Graphics. All data are presented as mean \pm standard error of the mean (SEM) unless mentioned otherwise. Statistical differences were determined using one-way ANOVA with a Bonferonni post hoc test. Significance was designated at p < 0.05. All statistical analysis and graphical depictions were carried out using OriginPro Software, version

2021 (OriginLab Corp., Northampton, MA) and Microsoft Excel.

■ RESULTS AND DISCUSSION

The electrochemistry of oxytocin has been previously studied using carbon macroelectrodes.³⁰ The oxidation of oxytocin occurs at the tyrosine moiety, the only electroactive amino acid presented in the oxytocin structure. The proposed mechanism involves one-electron oxidation and loss of a proton at the hydroxyl group of the phenol group (Figure 1).³⁰ The resulting

Figure 1. Proposed oxidation mechanism of oxytocin oxidation at the tyrosyl moiety. R and R' represent the remaining parts of oxytocin.

radical is highly reactive and susceptible to further nucleophilic attack, leading to polymerization and formation of a complex mixture of substances. Such polymerization results in subsequent adsorption of the reaction products on the electrode surface, leading to electrode fouling and a significant reduction of the electrode sensitivity. Traditionally, the FSCV waveform for the detection of electrochemically active analytes has employed a simple triangular shape (ranging from a holding potential of -0.4 V to a switching potential of 1.3 V and back at a scan rate of 400 V/s and frequency of 10 Hz, Figure 2A). However, using this waveform for the detection of peptides results in passivation of the electrode surface and loss of faradaic signal, as illustrated by the color plot (Figure 2A) and cyclic voltammograms at selected time points (Figure 2B).

To address this issue, Schmidt et al. introduced a modified sawhorse waveform that incorporated multiple scan rate steps that mitigate fouling upon oxidation of met-enkephalin, a pentapeptide that also possesses a tyrosine residue. This waveform incorporated a linear scan from -0.2 to +0.6 V at a rate of 100 V/s and then to +1.2 V at 400 V/s. After a 3 ms holding time, the potential was linearly decreased to -0.2 V at 100 V/s. Oxidation of the hydroxyl group was observed during the scan from +0.6 to +1.2 V. The higher scan rate increases the faradaic current measured, while holding the electrode at a potential above +1.1 V decreases the adsorption of tyrosine, thereby decreasing fouling. 33

Oxytocin Waveform Optimization. Key waveform parameters were optimized to maximize the faradaic current resulting from the oxidation of oxytocin. The investigated parameters include waveform application frequency, upper limit of the potential window, switching potential, and scan rate. Because oxytocin possesses tyrosine, the previously published modified sawhorse waveform was used as an initial starting point and further modified.

Waveform Frequency. Oxytocin possesses a positive charge at a physiological pH; thus, the negative holding potential between scans serves as a preconcentration step in which the positively charged peptide accumulates at the negatively charged electrode surface. Because changes in the waveform frequency alter the duration of this preconcentration step, we collected measurements at selected frequencies, with the remaining parameters held constant at the values used by Calhoun et al.²⁵

Figure 3A,B shows CVs resulting from this change in frequencies and the peak oxidation currents, respectively. Oxidation current decreased with increasing frequency and accumulation time (indicated in red at the top of Figure 3B), suggesting that oxytocin is preconcentrating at the electrode surface between scans. The negative shift in current that occurs while holding potential constant may be caused by a

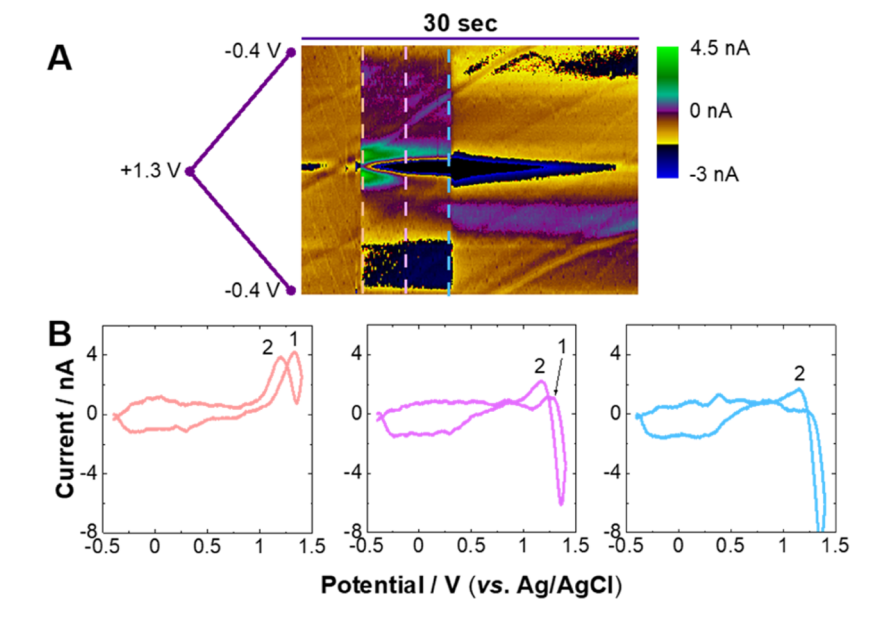


Figure 2. Oxytocin fouls the carbon-fiber microelectrode surface when the traditional FSCV waveform is used (holding potential -0.4 V, switching potential +1.3 V, scan rate 400 V/s, frequency 10 Hz). (A) Color plot representing the change in current as a function of time and applied potential. Oxytocin is injected at approximately 5.5 s, and the injection port is closed approximately at 13 s. (B) Voltammetric response for oxytocin is unstable over time. Representative CVs are shown for t = 5.6, 8.8, and 12.5 s. The oxidation peaks are labeled on the CVs.

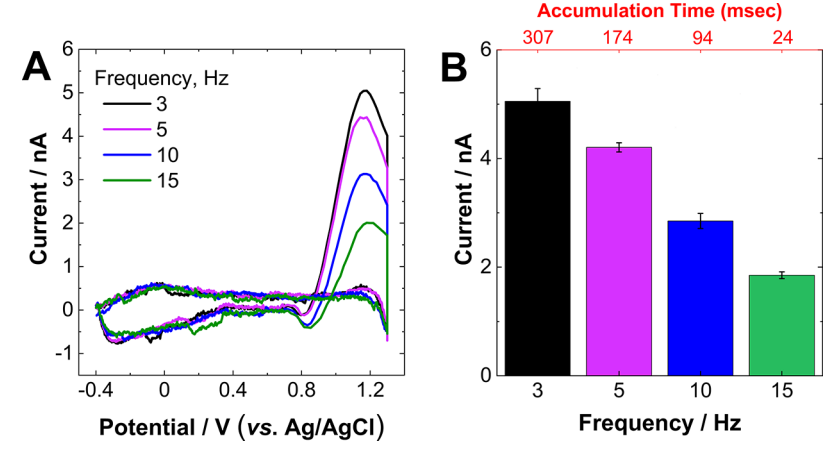


Figure 3. Waveform frequency affects sensitivity to oxytocin. (A) Representative voltammograms for 3 μ M oxytocin. (B) Peak oxidation current decreases with increasing frequency (decreasing accumulation time, respectively). One-way ANOVA revealed a significant effect of frequency on current (p < 0.05, n = 3 electrodes).

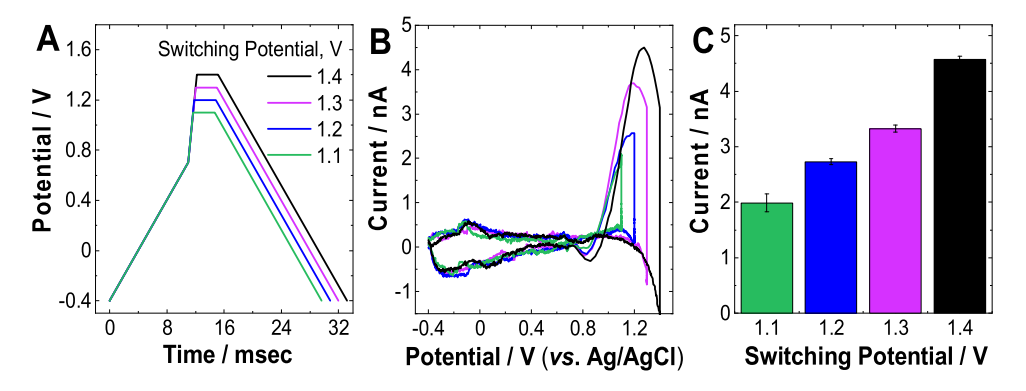


Figure 4. Oxytocin voltammetric response is dependent on the switching potential. (A) Schematic representation of the waveforms used for the investigation of the switching potential (from +1.1 to +1.4 V) on the oxytocin current response. (B) Representative voltammograms for 3 μ M oxytocin. A high switching potential (+1.4 V) is required for a well-defined oxidation peak. (C) Peak anodic potential increases as the switching potential increases (n = 3 electrodes).

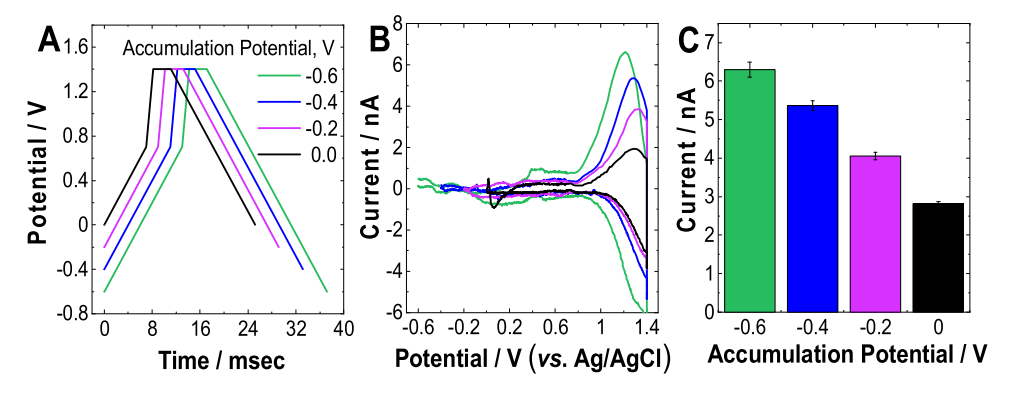


Figure 5. Oxytocin voltammetric response is dependent on the accumulation potential. (A) Schematic representation of the waveforms used for the investigation of the accumulation potential (from 0.0 to -0.6 V) on the oxytocin current response. (B) Representative voltammograms for 3 μ M oxytocin. (C) Peak oxidation potential increases as the holding potential decreases (n = 3 electrodes). One-way ANOVA revealed a significant effect of accumulation potential on current (p < 0.05).

combination of factors, including etching of the electrode surface and changes in the electric double layer from adsorption of oxytocin. More work is needed to elucidate particular contributions. The lowest frequency of 3 Hz resulted in the highest current as the maximum time was available for the adsorption at the holding potential. However, as a compromise between temporal resolution and sensitivity, 5 Hz was chosen as the optimal waveform frequency.

Switching Potential. The effect of switching potential on oxytocin current response was studied by obtaining CVs with selected switching potentials ranging from +1.1 to +1.4 V (Figure 4A). The representative CVs in Figure 4B reveal that the higher switching potentials of +1.3 and +1.4 V yielded well-defined oxidation peaks, while +1.1 and +1.2 V did not. In addition, the anodic peak current increased significantly with increasing switching potential, demonstrating higher sensitivity

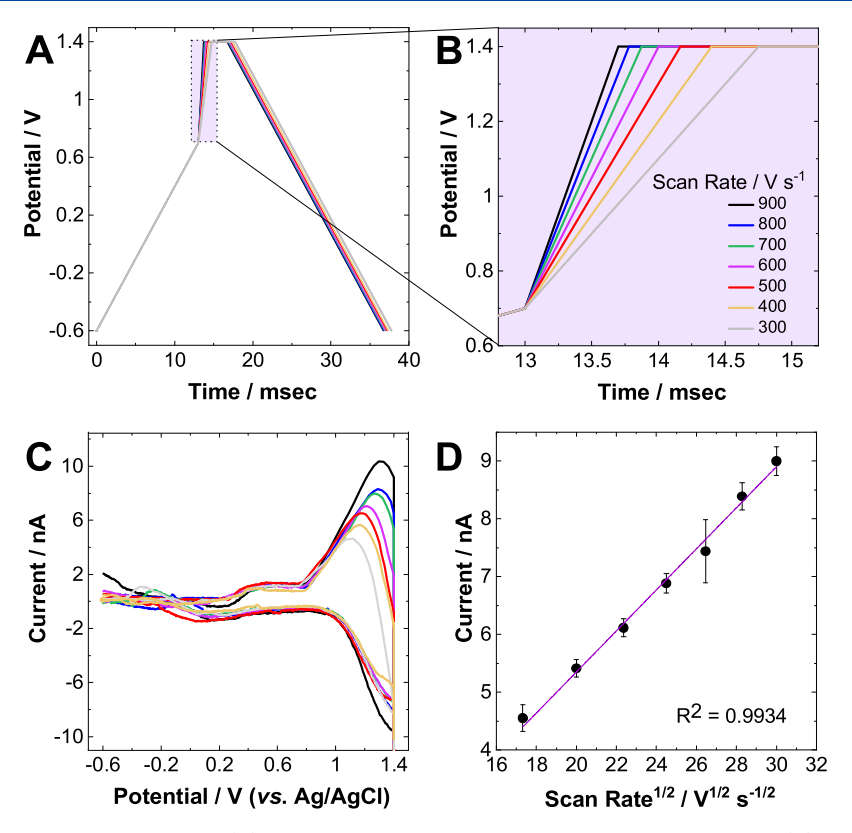


Figure 6. Effect of scan rate on oxytocin oxidation. (A) Graphical representation of the investigated waveforms. (B) Highlighted region of interest. (C) Cyclic voltammograms of 3 μ M oxytocin recorded as a response of scan rate from 300 to 900 V/s. The current response increased linearly as a function of both (D) square root of scan rate and (E) scan rate. Error bars represent mean \pm SEM (n=3 electrodes).

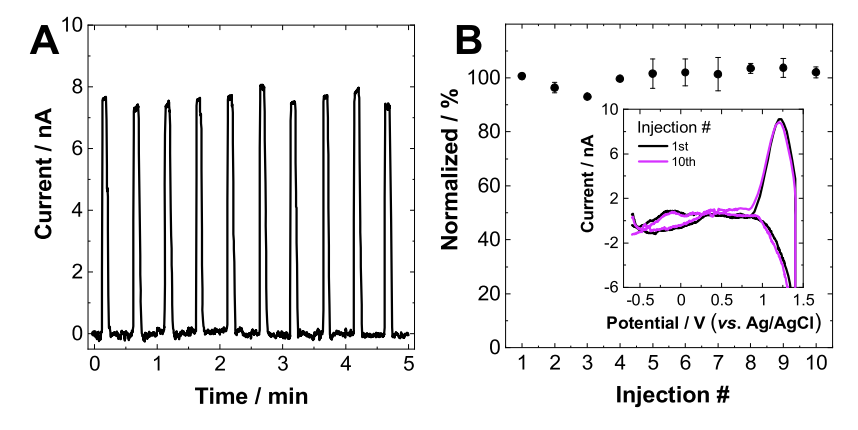


Figure 7. Electrode stability. Electrode fouling resistance was determined by injecting 3 μ M oxytocin 10 times every 40 s. (A) Current—time responses for a single electrode to illustrate the stability of the response. (B) Normalized current (to the first injection) with SEM error bars (n = 3 electrodes). RSD = 3.19 %, and there is no significant difference between the first and last injections. Inset: CVs for the first and last injections.

to oxytocin (p < 0.05; n = 3 electrodes). Therefore, the potential of +1.4 V was chosen as an optimal switching potential and further used for any consequent waveform optimization steps.

Accumulation Potential. The adsorption of oxytocin molecules, which are positively charged at a physiological pH, to the electrode surface occurs due to the negative holding potential. It is, therefore, a key waveform parameter due to its significant role in the preconcentration process. The amount of adsorbed analyte and, consequently, the measured current, should be affected by changes in the holding potential. To optimize this parameter, we obtained CVs using selected holding potentials ranging from 0.0 to -0.6 V (Figure 5A). More negative holding potentials resulted in significant

increases of peak current. The maximum oxidation signal was observed at -0.6 V; therefore, we chose this value for subsequent measurements.

Scan Rate. The kinetics of the electron transfer reaction were further investigated. According to the Randles–Sevcik equation, the faradaic current response increases linearly with the increasing square root of scan rate for diffusion-controlled reactions.³⁴ To study the nature of the oxytocin's interaction on the surface of the electrode, the scan rate was systematically varied from 200 to 900 V/s (Figure 6A,B), and the current response obtained from the resulting CVs was plotted as a function of the square root of scan rate (Figure 6C,D). The linearity of this plot ($R^2 = 0.9934$) suggests that the current measured is faradaic and diffusion-limited.

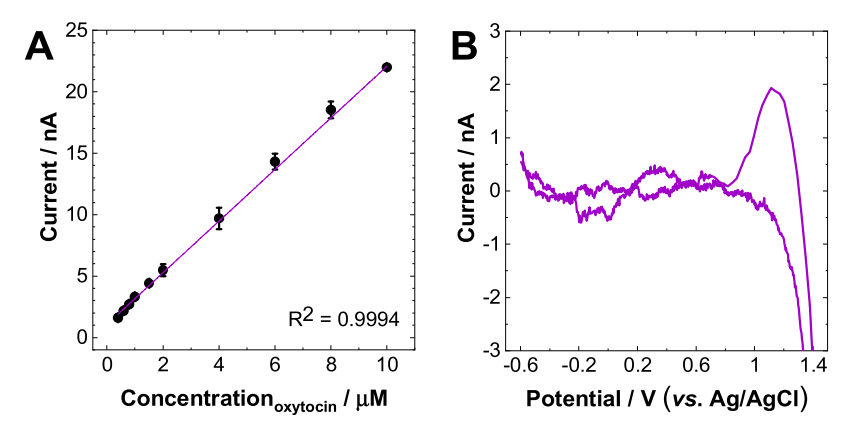


Figure 8. Detection of oxytocin using MSW exhibits nanomolar detection limits. (A) Calibration curve generated by flow injection analysis of increasing concentrations of oxytocin. (B) Representative CV for 0.4 μ M oxytocin demonstrates the ability for low concentration detection. Error bars represent mean \pm SEM (n = 3 electrodes).

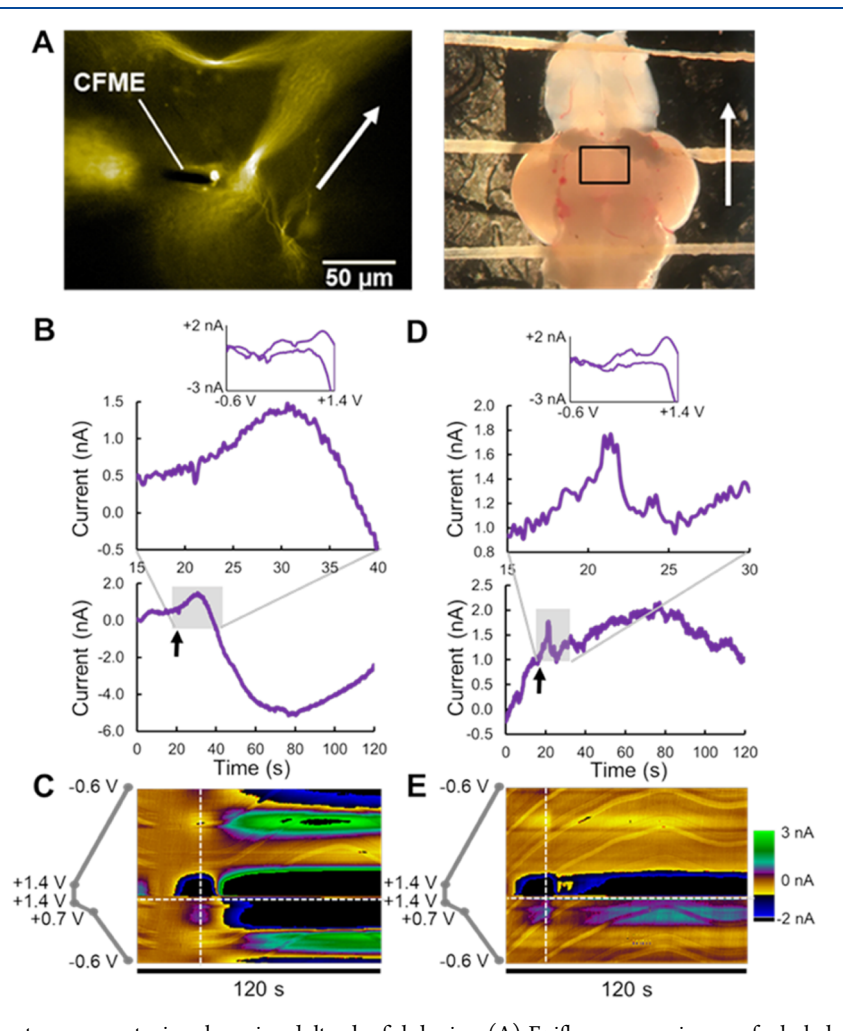


Figure 9. Stimulated and spontaneous oxytocin release in adult zebrafish brains. (A) Epifluorescence image of whole brain from adult *OXT-Gal4; UAS-ChREYFP* zebrafish (left) and bright-field image of zebrafish brain with approximate field of view in the left panel represented by the rectangle (right). The white arrows indicate relative orientation. Imaging (left): Nikon E600FN epifluorescence microscope Plan Fluor 40X/0.80 NA water immersion objective. (B, C) Current—time plots of light-induced oxytocin release and putative mechanically induced oxytocin release. Inset: CVs suggesting that the identity of measured species is oxytocin. The stimulated release is short term and is superimposed over longer-term oxytocin transient concentration changes. (C, E) Respective color plots of light- and mechanically evoked oxytocin release.

To determine the optimum scan rate value, both the current response and peak oxidation potential must be taken into consideration. As mentioned, the response current is increasing with increasing scan rate, providing the highest oxidation current at the rate of 900 V/s. However, at the fastest investigated scan rate (900 V/s), the oxidation peak occurred near the switching potential, suggesting that oxidation cannot be fully completed before scanning toward the negative

potential. As the scan rate decreases, the position of the oxytocin oxidation peak shifted to the less positive potential values, with a more defined peak shape. As a trade-off to providing a well-defined peak while also maximizing the oxidation current, we chose a scan rate of 600 V/s.

Electrode Stability. To measure oxytocin release consistently, it is necessary for the electrode to provide the same response over multiple measurements and extended periods of time. Electrode stability and resistance to fouling were investigated by applying repeated injections of 3 μ M oxytocin every 40 s by flow injection analysis, with a total of 10 injections (Figure 7A). To visualize any significant changes in current, the evaluated faradaic current was normalized to the first injection (Figure 7B). The current vs time record for 10 consecutive injections, as well as CVs of the first and last injections of oxytocin showed no significant degradation in peak current and/or change in the shape of the CV (Figure 7B, inset). The relative standard deviation (RSD) for 10 injections was 3.19%, indicating that the electrodes have good stability when applying this waveform. Furthermore, no trend showing the progressive decrease of the signal over time was observed, and the newly developed waveform for the detection of oxytocin did not foul the CFE surface when exposed to repeated oxytocin injections.

Oxytocin Limit of Quantitation. We generated a calibration curve for oxytocin using the optimized waveform by plotting the current response (collected at +1.15 V) and the analyte concentration ranging from 0.4 to 10 μ M (Figure 8). We found that the limit of quantitation, obtained at S/N = 10, was 0.34 \pm 0.02 μ M. Furthermore, regression analysis indicated a high degree of linearity (R^2 = 0.9994), indicating that the application of this optimized waveform can be used to quantitate the release of oxytocin at low concentrations.

Oxytocin Release in *Ex Vivo* **Zebrafish Brain.** To demonstrate the utility of our approach, we measured the light-evoked release of oxytocin in *ex vivo* whole brains harvested from transgenic zebrafish expressing fluorescently tagged channelrhodopsin-2 within oxytocinergic neurons (*Tg-[oxt:Gal4-VP16; uas:chr2-eyfp]*).

Figure 9A (left) shows an epifluorescence image of a carbonfiber microelectrode placed in the vicinity of oxytocinergic neurons, located in the preoptic nucleus of the hypothalamus. The overall orientation of the electrode placement is indicated in Figure 9A (right). After placing the electrode, we exposed the brain to a 200 ms pulse of ~480 nm light from a xenon lamp source. The current-time trace in Figure 9B shows a temporary increase in current. The current then dropped sharply. The CV (Figure 9B, top) was sampled at 30 s, and an averaged set of five background scans obtained at 15 s was subtracted from the entire set of CVs. The CV in Figure 9B closely resembles those obtained by flow injection analysis (e.g., Figure 8), suggesting that the current increase arises from oxytocin release. The average concentration of light-stimulated oxytocin release was estimated to be 0.40 \pm 0.04 nM (n = 3separate measurement locations in two brains).

Interestingly, in this plot, our stimulated release appears to be superimposed upon transient oxytocin release events, with the current decreasing below the initial baseline value, reaching a minimum at about 80 s, and then increasing. Further supporting the idea that these currents arise from the presence of oxytocin, the color plot current signal occurring after about 40 s resembles an inverse of the currents obtained at 30 s. We

have carried out multiple measurements in two other brains and have noted similar patterns of transient oxytocin release.

To our knowledge, the electrochemical measurement of oxytocin release directly from the brains of any organism has not been published in the peer-reviewed literature. Oxytocin has been measured *in vivo* from the paraventricular nucleus of anesthetized rats by microdialysis sampling with detection by liquid chromatography—mass spectrometry. Using this method, it was determined that the basal concentration of oxytocin in the microdialysates was 5.4 ± 1.3 pM and that this value increased 530% upon stimulation by injection of aCSF that contains 75 mM K⁺. Possible factors that contribute to the greater concentration determined by our methods (several orders of magnitude) include measurement of oxytocin levels directly at the site of the neurons on faster timescales, low oxytocin recoveries in the microdialysates, differences in stimulation regimens, and differences in species.

Next, we attempted stimulation by mechanically moving the microelectrode laterally \sim 5 μ m over \sim 0.5 s (Figure 9D,E). This method of stimulation had been applied previously to evoke adenosine release in brain tissue. We noted a sharp increase in current, suggesting that oxytocin release occurred. We also collected files in the absence of stimulation and found what appeared to be transient changes in oxytocin release that occurred over the course of seconds, like those superimposed on stimulated release currents in the dataset shown in Figure 9B,C. While it is possible that other electroactive components are released due to mechanical stimulation, it is important to note that a subpopulation of oxytonergic neurons in the hypothalamus is mechanosensitive. Thus, we speculate that oxytocin is likely present along with other tyrosine-containing peptides.

Stimulated and transient release from terminals that project to various brain regions as well as release from oxytocinergic cell bodies and dendrites (somatodendritic release) is known to occur in multiple species.^{37–39} The current we measured in zebrafish, given the location in the brain, arises possibly from somatodendritic release or from short-range axonal projections. It will be important to determine if the transients arise from our handling of the tissue (*e.g.*, application of light for imaging) or if they occur naturally.

CONCLUSIONS

In this research, we developed a waveform optimized for the measurement of oxytocin, a nonapeptide that is an important player in numerous biological functions. However, it is difficult to measure because it tends to foul the carbon-fiber electrode surface. We also demonstrated the measurement of oxytocin in genetically altered zebrafish that express channelrhodopsin and yellow fluorescent protein selectively in oxytocinergic neurons. Our findings demonstrate that we can measure stimulated release as well as spontaneously occurring oxytocin transients. In the future, it will be important to further validate our method in more complex species, including rodents.

ASSOCIATED CONTENT

Supporting Information

The Supporting Information is available free of charge at https://pubs.acs.org/doi/10.1021/acs.analchem.1c04879.

Alternative representation of data and current plotted against time for a typical cyclic voltammogram (PDF)

AUTHOR INFORMATION

Corresponding Author

Michael A. Johnson – Department of Chemistry and R.N. Adams Institute for Bioanalytical Chemistry, University of Kansas, Lawrence, Kansas 66045, United States;

orcid.org/0000-0001-5078-9896; Phone: 785-864-4269; Email: johnsonm@ku.edu

Authors

Romana Jarosova — Department of Chemistry and R.N. Adams Institute for Bioanalytical Chemistry, University of Kansas, Lawrence, Kansas 66045, United States; Department of Analytical Chemistry, UNESCO Laboratory of Environmental Electrochemistry, Charles University, Prague 2 12843, Czech Republic; Present Address: University of Cincinnati, Cincinnati, Ohio 45221, United States

Adam D. Douglass – Department of Neurobiology and Anatomy, University of Utah, Salt Lake City, Utah 84112, United States

Complete contact information is available at: https://pubs.acs.org/10.1021/acs.analchem.1c04879

Author Contributions

M.A.J. and R.J. conceived all experiments. R.J. performed all experiments. A.D.D. developed and supplied Tg[oxt:Gal4-VP16; uas:chr2-eyfp]. The manuscript was written through contributions of all authors. All authors have given approval to the final version of the manuscript.

Notes

The authors declare no competing financial interest.

ACKNOWLEDGMENTS

Support for this research was provided by grants from the National Institutes of Health, R21NS109659 (MAJ), P20GM103638 (MAJ), and R01NS111067-01 (ADD); the University of Kansas (MAJ); the National Science Foundation, IOS10043082 (ADD); and Charles University in Prague under Award Number SVV260560 (RJ).

REFERENCES

- (1) Mauri, A.; Argiolas, A.; Ticconi, C.; Piccione, E. Reprod., Fertil. Dev. 1995, 7, 1481–1484.
- (2) Drewett, R. F.; Bowen-Jones, A.; Dogterom, J. Horm. Behav. 1982, 16, 245-248.
- (3) Liu, Y.; Wang, Z. X. Neuroscience 2003, 121, 537-544.
- (4) Ogi, A.; Mariti, C.; Pirrone, F.; Baragli, P.; Gazzano, A. Animals **2021**, 11, No. 1130.
- (5) Oti, T.; Sakamoto, T.; Sakamoto, H. Commun. Integr. Biol. 2021, 14, 55–60.
- (6) Kosfeld, M.; Heinrichs, M.; Zak, P. J.; Fischbacher, U.; Fehr, E. *Nature* **2005**, 435, 673–676.
- (7) Smith, A. S.; Wang, Z. Biol. Psychiatry 2014, 76, 281-288.
- (8) Zimmerman, E. A.; Nilaver, G.; Hou-Yu, A.; Silverman, A. J. Fed. Proc. 1984, 43, 91–96.
- (9) Gimpl, G.; Fahrenholz, F. Physiol. Rev. 2001, 81, 629-683.
- (10) Rossoni, E.; Feng, J.; Tirozzi, B.; Brown, D.; Leng, G.; Moos, F. *PLoS Comput. Biol.* **2008**, 4, No. e1000123.
- (11) Love, T. M. Pharmacol., Biochem. Behav. 2014, 119, 49-60.
- (12) Flight, M. H. Nat. Rev. Neurosci. 2013, 14, 740-741.
- (13) Tyzio, R.; Nardou, R.; Ferrari, D. C.; Tsintsadze, T.; Shahrokhi, A.; Eftekhari, S.; Khalilov, I.; Tsintsadze, V.; Brouchoud, C.; Chazal, G.; Lemonnier, E.; Lozovaya, N.; Burnashev, N.; Ben-Ari, Y. *Science* **2014**, 343, 675–679.

- (14) Yoshimura, R.; Kiyama, H.; Kimura, T.; Araki, T.; Maeno, H.; Tanizawa, O.; Tohyama, M. *Endocrinology* **1993**, *133*, 1239–1246.
- (15) de Moura Oliveira, V. E.; Lukas, M.; Wolf, H. N.; Durante, E.; Lorenz, A.; Mayer, A. L.; Bludau, A.; Bosch, O. J.; Grinevich, V.; Egger, V.; de Jong, T. R.; Neumann, I. D. *Nat. Commun.* **2021**, *12*, No. 2900.
- (16) Landgraf, R.; Neumann, I.; Russell, J. A.; Pittman, Q. J. Ann. N. Y. Acad. Sci. 1992, 652, 326–339.
- (17) Gozdowska, M.; Kulczykowska, E. J. Chromatogr. B: Anal. Technol. Biomed. Life Sci. 2004, 807, 229–233.
- (18) Mabrouk, O. S.; Kennedy, R. T. J. Neurosci. Methods 2012, 209, 127–133.
- (19) Wang, L.; Marti, D. W.; Anderson, R. E. Molecules 2019, 24, 3079.
- (20) Kendrick, K. M. J. Neurosci. Methods 1990, 34, 35-46.
- (21) Lin, C. Y.; Tsai, S. H.; Tai, D. F. J. Pept. Sci. 2019, 25, No. e3150.
- (22) Lane, R. F.; Hubbard, A. T. Anal. Chem. 1976, 48, 1287-1292.
- (23) Schmidt, A. C.; Dunaway, L. E.; Roberts, J. G.; McCarty, G. S.; Sombers, L. A. *Anal. Chem.* **2014**, *86*, 7806–7812.
- (24) Shen, H.; Lada, M. W.; Kennedy, R. T. J. Chromatogr. B: Biomed. Sci. Appl. 1997, 704, 43-52.
- (25) Calhoun, S. E.; Meunier, C. J.; Lee, C. A.; McCarty, G. S.; Sombers, L. A. ACS Chem. Neurosci. 2019, 10, 2022–2032.
- (26) Kraft, J. C.; Osterhaus, G. L.; Ortiz, A. N.; Garris, P. A.; Johnson, M. A. Neuroscience 2009, 161, 940–949.
- (27) Landin, J.; Hovey, D.; Xu, B.; Lagman, D.; Zettergren, A.; Larhammar, D.; Kettunen, P.; Westberg, L. Sci. Rep. 2020, 10, 5435.
- (28) Nagel, G.; Brauner, M.; Liewald, J. F.; Adeishvili, N.; Bamberg, E.; Gottschalk, A. Curr. Biol. 2005, 15, 2279–2284.
- (29) Wee, C. L.; Nikitchenko, M.; Wang, W. C.; Luks-Morgan, S. J.; Song, E.; Gagnon, J. A.; Randlett, O.; Bianco, I. H.; Lacoste, A. M. B.; Glushenkova, E.; Barrios, J. P.; Schier, A. F.; Kunes, S.; Engert, F.; Douglass, A. D. *Nat. Neurosci.* **2019**, *22*, 1477–1492.
- (30) Asai, K.; Ivandini, T. A.; Einaga, Y. Sci. Rep. 2016, 6, No. 32429.
- (31) Jackson, B. P.; Dietz, S. M.; Wightman, R. M. Anal. Chem. 1995, 67, 1115–1120.
- (32) Cooper, S. E.; Venton, B. J. Anal. Bioanal. Chem. **2009**, 394, 329–336.
- (33) Ogura, K.; Kobayashi, M.; Nakayama, M.; Miho, Y. J. Electroanal. Chem. 1999, 463, 218–223.
- (34) Bard, A. J.; Faulkner, L. R. Electrochemical Methods: Fundamentals and Applications; 2nd ed.; John Wiley & Sons, Ltd., 2000
- (35) Wang, Y.; Venton, B. J. Neurochem. Int. 2019, 124, 46-50.
- (36) Wee, C. L.; Nikitchenko, M.; Wang, W. C.; Luks-Morgan, S. J.; Song, E.; Gagnon, J. A.; Randlett, O.; Bianco, I. H.; Lacoste, A. M. B.; Glushenkova, E.; Barrios, J. P.; Schier, A. F.; Kunes, S.; Engert, F.; Douglass, A. D. *Nat. Neurosci.* **2019**, *22*, 1477–1492.
- (37) Althammer, F.; Eliava, M.; Grinevich, V. Handb. Clin. Neurol. **2021**, 180, 25-44.
- (38) Ludwig, M.; Stern, J. Philos. Trans. R. Soc., B 2015, 370, No. 20140182.
- (39) Pow, D. V.; Morris, J. F. Neuroscience 1989, 32, 435-439.